Teknik Dergi, 2021 11381-11405, Paper 638

Experimental Study on the Behavior of Header End - Plate Connections under Cyclic Loading

Adem KARASU[1]
Cüneyt VATANSEVER[2]

ABSTRACT

This paper presents the results from an experimental study on the actual behavior of header end-plate connections. To better understand the hysteretic behavior of these connections in terms of the stiffness and the strength, sixteen specimens were considered and subjected to cyclic loads. The effect of some parameters such as thickness of the header end-plate, depth of the connection and the number of bolt rows on the behavior of header end-plate connections has been investigated by the help of experimental tests and finite element (FE) analyses. The moment-rotation relations of the connections governed by three parameters such as initial stiffness, moment capacity and rotation capacity were obtained. Results revealed that the moment capacity increases with the increase in end-plate thickness and depth of connection. However, for the equal connection depth, increasing the number of bolt rows has not influenced the connection behavior in any noticeable way.

Keywords: Steel structures, semi-rigid connections, header end-plate, experimental study, finite element method.

1. INTRODUCTION

The use of bolted end-plate connections has become popular due to ease of fabrication, erection and proper seismic behavior. After the 1994 Northridge earthquake, bolted end-plate connections have seen a rise in popularity as engineers seek alternatives to the welded connections. Moreover, these connections exhibited more suitable results than rigid welded connections (Chen et al. [1]). These connections have the advantage of less supervision and shorter assembly time than welded connections.

Research in bolted end-plate connections provided liability of bolted extended and flush end-plate connections to serve as moment resisting connections. One of them presented by Sherif

Note:
- This paper was received on January 14, 2020 and accepted for publication by the Editorial Board on May 23, 2020.
- Discussions on this paper will be accepted by January 31, 2022.

• https://dx.doi.org/10.18400/tekderg.674889

1 Istanbul Technical University, Department of Civil Engineering, Istanbul, Turkey - karasuad@itu.edu.tr https://orcid.org/0000-0002-1063-8484

2 Istanbul Technical University, Department of Civil Engineering, Istanbul, Turkey - cuneyt.vatansever@itu.edu.tr - https://orcid.org/0000-0002-9954-925X

et al. [2] and Bing et al. [3] have studied cyclic behavior of flush end-plate and extended end-plate connections, respectively. Cyclic behavior of bolted extended end-plate connections was evaluated and responses of the specimens were examined in ABAQUS software presented by Ismail et al. [4] and Haghollahi and Jannesar [5]. Fang et al. [6] has investigated the cyclic performance of extended end-plate connections equipped with shape memory alloy (SMA) bolts numerically and experimentally. It was clearly observed from the test results that longer SMA bolts resulted in higher ductility. Dessouki et al. [7], Adey [8] and Johnstone and Walpole [9] have used the yield line theory to propose equations for the four bolts and multiple row extended end-plate connections. However, limited number of experimental investigations in the area of cyclic behavior of header end-plate connections has been carried out.

Header end-plate connection is a kind of bolted end-plate connection whose length is less than the depth of the beam. Since they have limited stiffness and strength, these types of connections are also called a shear end-plate connection in the AISC-LRFD specifications [10] and fall in the category of flexible connections (Kishi et al. [11]). Moment-rotation characteristics of these type of steel connections are indicative of the connection's stiffness, strength and ductility. Stiffness, strength and ductility of the connections are believed to be critical factors for structures located in seismic areas. Furthermore, in seismic design, the flexible semi-rigid connections might be alternatively employed to offer sufficient plastic rotations. Jaspart and Demonceau [12] presented design sheets that contain practical ways to satisfy the ductility and rotation requirements of header end-plate connections.

A joint may be classified as full-strength, nominally pinned or partial strength by comparing moment resistance, and can be categorized as fully-rigid, nominally pinned or semi-rigid according to its initial rotational stiffness according to Eurocode (EN 1993-1-8, [13]). The design of joints within this partial strength/semi rigid approach is becoming more and more popular, because actual behavior of the connections significantly influence the distribution of the internal forces and overall deformations of the structure. Therefore, the studies on header end-plate connections have concentrated on experimental tests and analytical studies for achieving the moment-rotation relations (Sommer [14], Aggarwal [15], Pilgr [16]) under monotonic loading.

Most of the experimental studies were conducted on monotonic loading on header end-plate connections. The lack of cyclic test results of header end-plate connections motivated the study presented in the paper. That is the reason why the hysteretic response of this type of connection must be investigated to better understand the behavior of structural system under seismic loads when these connections are used as a beam-to-column connections. In this study, therefore, we experimentally investigated the nonlinear behavior of bolted header end-plate connections under cyclic loading. The behavior of the bolted header end-plate steel connections is entirely dependent upon and highly sensitive to the connection's geometric variables. It is essential that the influence of these parameters on the performance of header end-plate connections must be investigated to make proper assessment. The studied parameters were as follows: end-plate thickness, depth of the connection and number of bolt rows. Also, we examined the applicability of these connections according to AISC provisions (AISC341-16, [17]) by presenting moment-rotation hysteretic response of the connections. Thus, it may be possible to provide a contribution to the energy dissipated during the

earthquake, if gravity frames with these connections are used combining with the special moment frames.

2. EXPERIMENTAL PROGRAM

2.1. Test Specimens

The study included a total of sixteen full scale tests that were performed in the Structural and Earthquake Engineering Laboratory of Istanbul Technical University. Two specimens with the characteristics of T5-20, whose details will be described later, were prepared and one of these was used in the pilot test to ensure that the test setup worked properly. Pilot test results are identical to the test results mentioned in the paper for the other specimen of T5-20. An extensive parametric study was conducted with the different configurations of end-plate as shown in Figure 1. The main test parameters for header end-plate connections were end-plate thickness, depth of the connection and number of bolt rows. Each specimen consisted of a column and a cantilever beam connected to the column flange at column's mid-height. The length of the column was 3020 mm and the length of the beams were 1760 mm, 1755 mm and 1750 mm, respectively. As for the end-plate thicknesses; 10 mm, 15 mm and 20 mm were considered. M20 high strength bolts of grade 10.9 (yield strength, F_{yb} is 900 N/mm^2, tensile strength, F_{ub} is 1000 N/mm^2) were employed for the connections. All bolts were fully tightened to the specified pretension force of 172 kN (TCDCSS, [18]) which is defined as the minimum pretension force for M20-10.9 bolts, using a torque wrench previously calibrated for each specimen. The bolts had the same dimensions and different arrangements for each type of the connection, as illustrated in Figure 1. The beam web was attached to the end-plate with double-sided fillet welds. For the current study the column and its flange were designed to have negligible deformation. Stiffener plates with a thickness of 10 mm were also placed between the column flanges on both sides of the column web at the level of beam flanges to limit the bending deformation of the column flange. The throat size of the fillet weld used for connecting beam web to end-plate was 10 mm and 6 mm fillet weld throat size was used for the stiffener connection to beam and column for all specimens. Because the moment resistance of the connection varies significantly to the depth of the end-plate, it was varied from 180 mm to 240 mm. The moment resistance of the connection is also affected by the number of bolts. Therefore, bolt rows changing from two to four were considered.

The tests were set-up using hot rolled European steel sections. To obtain the material characteristics of steel for each individual member involved in the connections, tensile tests were conducted considering three coupons for each member. For beams' (IPE 300) materials, all coupons were extracted from the web of IPE 300 profiles and as for columns (HEB 300) one coupon was cut from the flange, other two were extracted from the web. In total, 21 coupons were considered and average values for yield stress and elastic modulus are listed in Table 1. The results show that the experimental values were higher than the specified values of yield strength F_y as expected.

The naming convention used for the sample identification (TX-Y) is a combination of the type of the end-plate configurations (TX) and the thickness of the end-plate (Y) in mm. For example, a test designation of T3-20 indicates that the type of connection configuration is T3 and the thickness of the end-plate is 20 mm. Joint details for type 3 (T3-10,15,20) are given in Figure 2.

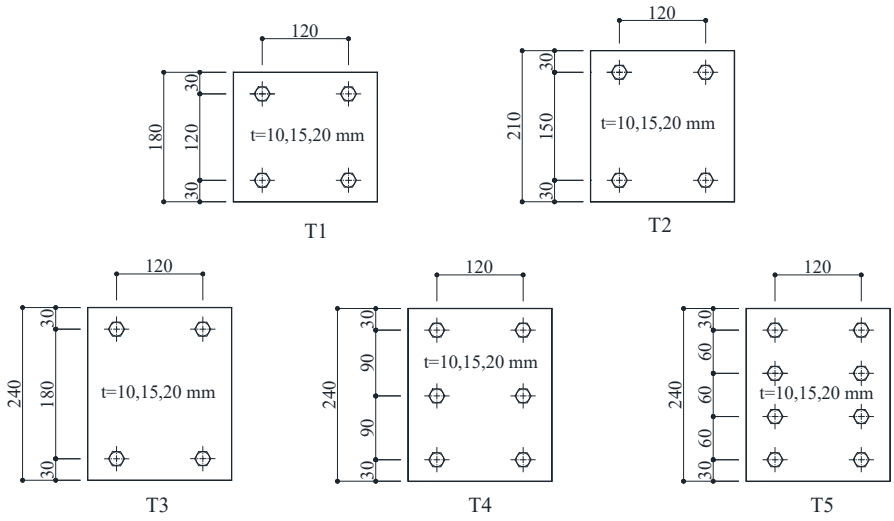

Figure 1 - Different header end-plate configurations

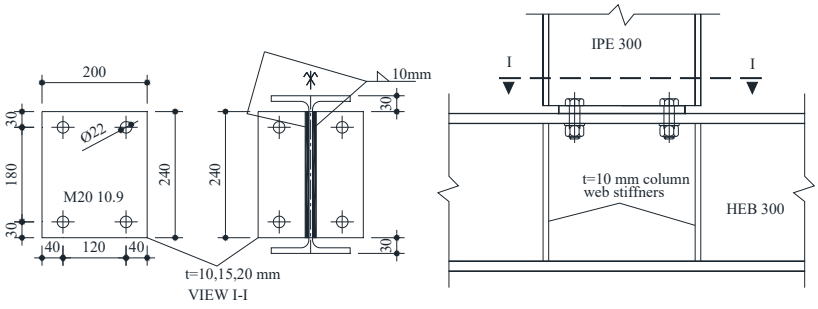

Figure 2 - Details of header end-plate connections for T3

Table 1 - Coupon test results

Specimen		F_y (N/mm^2)	F_u (N/mm^2)	E (N/mm^2)
End plate thickness t=10mm T(1,2,3,4,5)-10	Endplate t=10 mm (S235)	287.08	419.88	203316.66
	Beam / IPE 300 (S275)	325.03	442.91	205392.00
	Column / HEB 300 (S275)	346.88	478.80	205568.00
End plate thickness t=15mm T(1,2,3,4,5)-15	Endplate t=15 mm (S235)	280.35	392.09	194955.00
	Beam / IPE 300 (S275)	300.54	425.37	214514.00
	Column / HEB 300 (S275)	346.89	478.80	205568.00

Table 1 - Coupon test results (continue)

Specimen		F_y (N/mm^2)	F_u (N/mm^2)	E (N/mm^2)
End plate thickness t=20mm T(1,2,3,4,5)-20	Endplate t=20 mm (S235)	278.29	415.03	198171.66
	Beam / IPE 300 (S275)	332.95	470.80	208492.00
	Column / HEB 300 (S275)	346.89	478.80	205568.00

2.2. Test Setup and Instrumentations

Test setup and instrumentation used in the present study are shown in Figure 3. The test setup consists of a servo-controlled MTS hydraulic actuator with the loading capacity of ± 250 kN, stroke capacity of ± 300 mm and steel posts mounted on the strong floor. A load cell installed in the hydraulic actuator to measure the cyclic load. The column was connected to the supports via a pin connection using two rollers at both sides. It was assumed that the column is pin supported at mid-story. Also the length of the cantilever beam was considered more than five times the depth of the beam section that is exactly sufficient to idealize the flexural behavior. Besides, out of plane movement of the beam was prevented by using support frame, as seen in Figure 4.

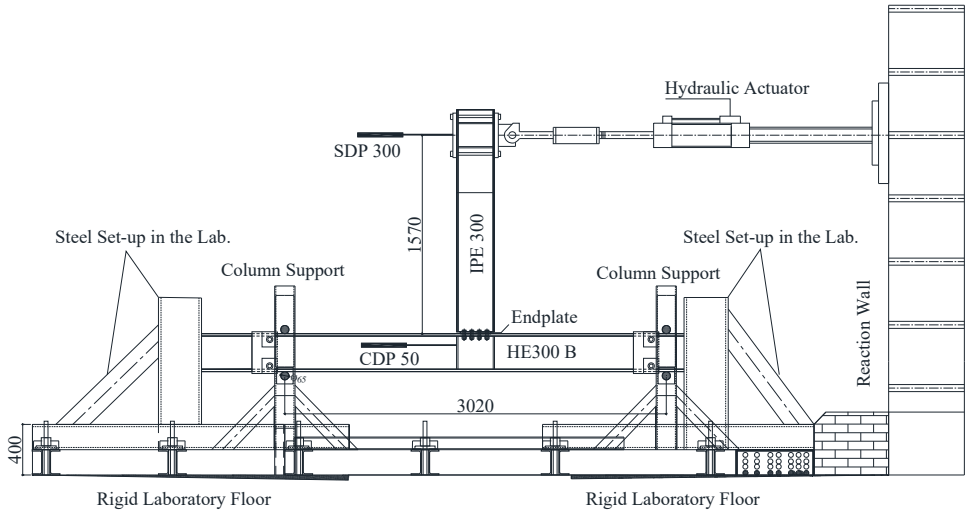

Figure 3 - The experimental setup

Linear variable differential transformers (LVDTs) were employed to measure lateral displacements of the beam and deformations of the connection during the tests. Strain gauges were placed on the end-plate and beam web at the connection, as shown in Figure 5, to determine the stress distribution and to monitor the progress of plasticity of the connection. The positions of the strain gauges were chosen at the positions of the expected maximum tensile strains as predetermined by the FE analyses results. One LVDT (SDP 300) was placed

to measure the top displacement at 1570 mm above the column flange surface. The other LVDT (CDP 50) was used to measure possible slippage of the specimen. The relative displacement of the beam top was calculated by deducting the horizontal displacement of the column from the total displacement of the beam top.

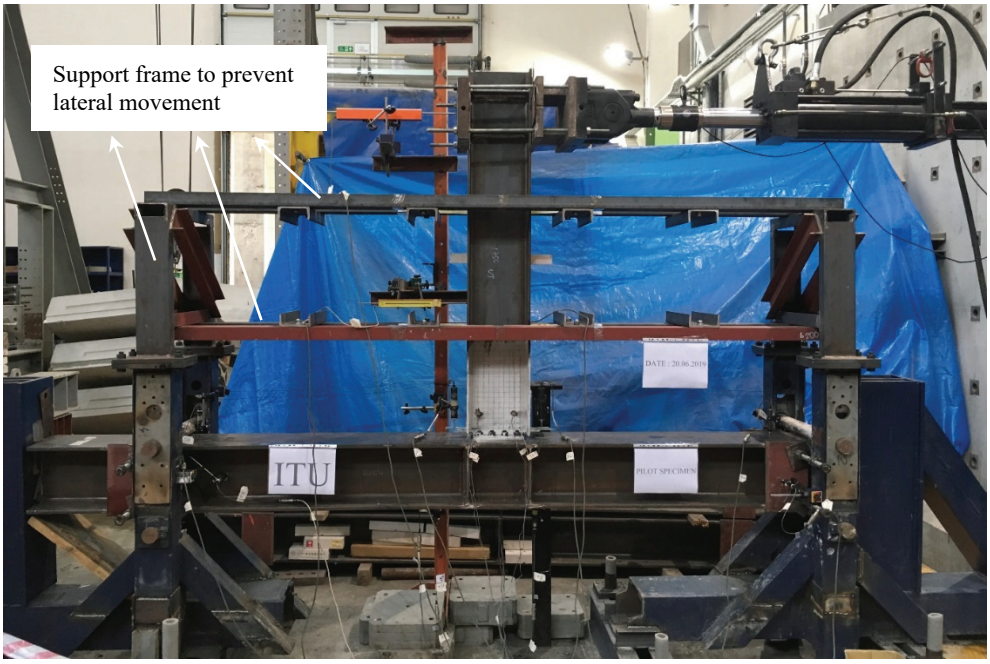

Figure 4 - Photographic view of the test setup

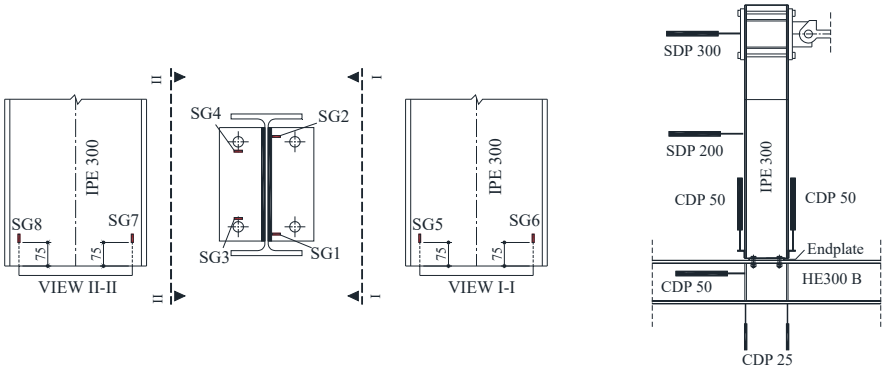

Figure 5 - Strain gauges and LVDT layout

2.3. Test Procedure

As previously described, to ensure a sufficient initial stiffness, full pretension was applied to each bolt. After bolt pretension process, the cyclic load was applied by the hydraulic jack at the beam top using a displacement control procedure. The loading protocol recommended by AISC (AISC341-16, [17]) was followed (Figure 6). This protocol uses drift angle, θ_b (relative displacement of beam divided by arm length (1570 mm)) as the main parameter, and the sequence of loading drifts are: 0.00375 (six cycles), 0.005 (six cycles), 0.0075 (six cycles), 0.01 (four cycles), 0.015 (two cycles), 0.02 (two cycles), 0.03 (two cycles), 0.04 (two cycles) and subsequent loadings at increments of θ_b=0.01 rad, with two cycles of loading at each step. For each loading, a set of readings were taken for displacement and applied load.

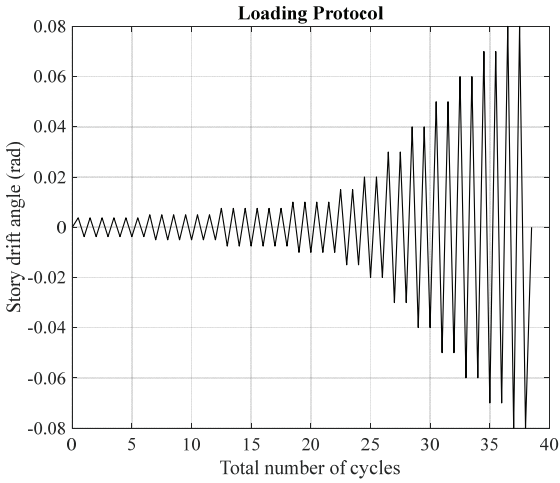

Figure 6 - Loading protocol

3. TEST RESULTS AND DISCUSSION

During the loading process, the shear action was well resisted via the friction between the end-plate and column flange face with no slippage observed. The bending moments at the connection are calculated by multiplying the load at the actuator with the distance to the column flange face. The failure conditions were considered to have reached when an abrupt or significantly large reduction occurred in the moment capacity.

The study mainly identified three types of behavior for the header end-plate connections. First, thin plate behavior where the end-plate is weaker and yields before the yielding and rupture of the beam web, secondly, intermediate plate behavior in which the end-plate and beam web plastify simultaneously and so both of them yield together, and finally thick plate behavior where the end-plate is stronger than the beam web and therefore, the beam web governs the flexural strength. According to the test results, increasing the number of bolt rows has negligible effect on the flexural capacity of the connections with thick plate, where the failure is governed by the beam web rupture. For these types of connections the test of each specimen was terminated after the rupture of the beam web. Experimental results are

summarized in Table 2, in which R_i, M_{max}, θ_{max} are the initial stiffnesses of the connections, the maximum moments achieved in the tests and the maximum rotations of the connections attained at the moment of the failure in the tests, respectively. Initial stiffnesses of the connections were determined by regression analysis considering a few data points in elastic region. The effect of each parameter on the connection behavior is assessed in the following sections.

Table 2 - Summary of the test results

	R_i (kNm/rad)	M_{max} (kNm)	θ_{max} (rad)	Failure Mode
T1-10	5494.0	18.44	0.09	End-plate tearing
T1-15	5471.1	35.51	0.08	End-plate tearing
T1-20	6179.3	41.69	0.04	Rupture of beam web
T2-10	7078.0	24.75	0.08	End-plate tearing
T2-15	7386.0	45.51	0.09	End-plate tearing
T2-20	8355.0	53.49	0.03	Rupture of beam web
T3-10	9667.1	29.62	0.07	End-plate tearing
T3-15	9792.9	57.89	0.09	End-plate tearing
T3-20	9755.6	67.98	0.02	Rupture of beam web
T4-10	9481.3	34.77	0.08	End-plate tearing
T4-15	10122	63.11	0.09	End-plate tearing
T4-20	9402.2	69.33	0.03	Rupture of beam web
T5-10	8962.9	38.90	0.08	End-plate tearing
T5-15	9825.2	64.44	0.08	Both End-plate tearing and Rupture of beam web
T5-20	9708.5	64.98	0.02	Rupture of beam

3.1. End-Plate Thickness

For the purpose of the discussion of the test results, the connection moment versus rotation hysteretic loops of all types of the connections are plotted in the same graph, as shown in Figure 7, to distinguish the behavior of the connections according to the end-plate thicknesses. As understood from the figures, the connections with the end-plates of 10 mm and 15 mm thicknesses exhibit more ductile behavior than those with the end-plates of 20 mm thickness because the flexural yielding of the end plate governs the behavior, which is defined as thin plate behavior. Moreover, the flexural capacities of the connections with 15 mm thick end-plate increase by about 70-100% when compared to those of the connections with 10 mm thick end-plate. Due to damage with the ductile tearing of the end-plate adjacent to the fillet welds, strength deterioration was observed at large rotations for 10 mm and 15 mm thick end-plates. Then, further increase in the end-plate thickness from 15 mm to 20 mm

has a little effect on the connection capacity as the behavior turns into the thick plate behavior. Furthermore, the ductility of the thicker end-plate connections is smaller than that of the other connections since the beam web in tension controls the behavior, which is described as the thick plate behavior.

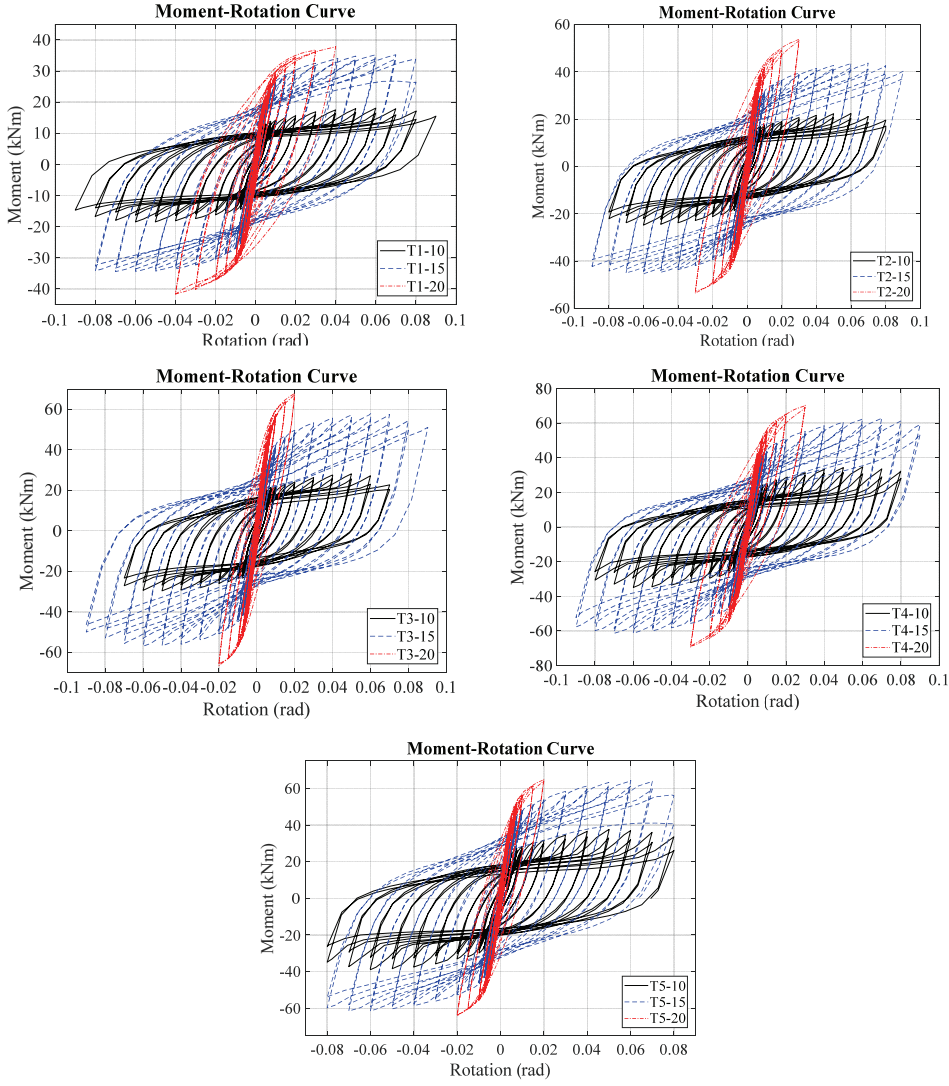

Figure 7 - Moment-rotation hysteretic loops

As seen from the Figure 7, the hysteretic loops are stable and the connections behave in a stiff linear manner at the beginning of the loading till reaching yield strength of either end-plate or beam web. Increasing the end-plate thickness has not significantly affected the initial

stiffness of the connections due to beam web playing a governing role in the elastic region. After yielding, the behavior becomes non-linear because of the plastic deformations occurred in both beam web and end-plate. It is apparent that end-plate thickness affects the behavior of the header end-plate connections significantly. According to the test results, specimens with end-plates of t=10 mm and t=15 mm show a higher ductility level while the specimen with the end-plate of t=20 mm develops the largest moment capacity with limited ductility. In these connections (t=20mm), further deformations cause the beam web to enter the inelastic range that leads to stiffness deterioration. For the connections with t=15 mm, the occurrence instant of the tearing of the end-plate together with the fracture of the beam web was so close as it would not recognize which one was earlier than the other for the specimens.

According to the observations during the tests shown in Figure 8, the connection with 10mm thick end-plate (relatively thin end-plate) reached the flexural capacity with the plastification of the end-plate. The flexural strength of the connection with 15mm thick end-plate (intermediate end-plate) was reached by yielding of both end-plate and the beam web while the yielding of the beam web governed the flexural capacity of the connection having 20mm thick plate (relatively thick end-plate). One indication that shows the flexural deformation of the end-plate is the amount of the separation observed between the surfaces of the end-plate and the column flange at the contact surface. As shown in the Figure 8, the sizes of the separations that took place at the connections with relatively thinner end-plates were larger than others with thicker ones. Spalling of whitewash, as seen in Figure 8 within the connection with 15 mm and 20 mm thick end-plate, indicates that the beam web yields. Strain gauge readings (S7) shown in Figure 9 also showed yielding occurred within the beam web. However, neither strain gauge readings (S5, S6, S7 and S8) nor observations during the test showed that the beam web of the specimen having 10mm thick header end-plate yields. Failure of the connection with the end-plate of 20mm thick occurred by rupture of the beam web adjacent to the fillet welds before the end-plate experienced sufficient flexural deformation to ensure ductility and rotational capacity. Therefore, the connection had relatively limited ductility and exhibited limited rotation capacity. Also, the parallel yield lines were observed at both bolt line and beam web-end-plate junction in addition to diagonal yield lines due to complete yielding of the end-plate of the specimen T5-10 and T5-15, while no complete yielding occurred in the end-plate of the specimen T5-20, as shown in Figure 10.

T5-10 T5-15 T5-20

Figure 8 - Failure modes of the samples

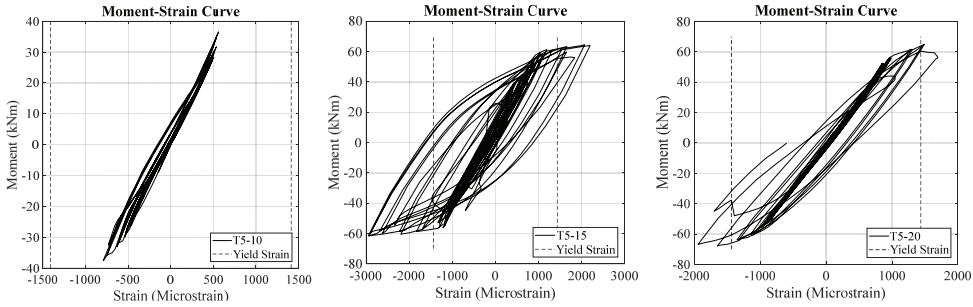

T5-10 T5-15 T5-20

Figure 9 - Moment-Beam web strain curves for T5 samples (S7)

Figure 10 - End-plate deformations (left to right; T5-10, T5-15, T5-20)

At the completion of tests, it was observed that effect of the prying forces that induced moment on bolt in addition to tensile forces, were more remarkable on the bolts in the connection with the end-plate of t=15mm than that with the end-plate of t=20mm due to larger flexural deformation of the end-plate occurred transversely. As seen in Figure 11, it is clear that the thicker the end-plate becomes, the smaller is the effect of the prying action .

T3-15 T3-20

Figure 11 - Deformed shape of the bolts

3.2. Depth of the Connection

As the depth of the end-plate increases from 180 mm to 240 mm, moment capacity of the connections is increased by about 60-65% for thin, intermediate and thick plates as shown in Figure 12. This is because the use of deep end-plate has developed longer lever-arm. Besides, a long lever-arm tends to reduce the connection rotation capacity as more applied load is needed to develop high moment resistance. Therefore the rotation capacity of the connection was less for deep end-plates than shallow end-plate.

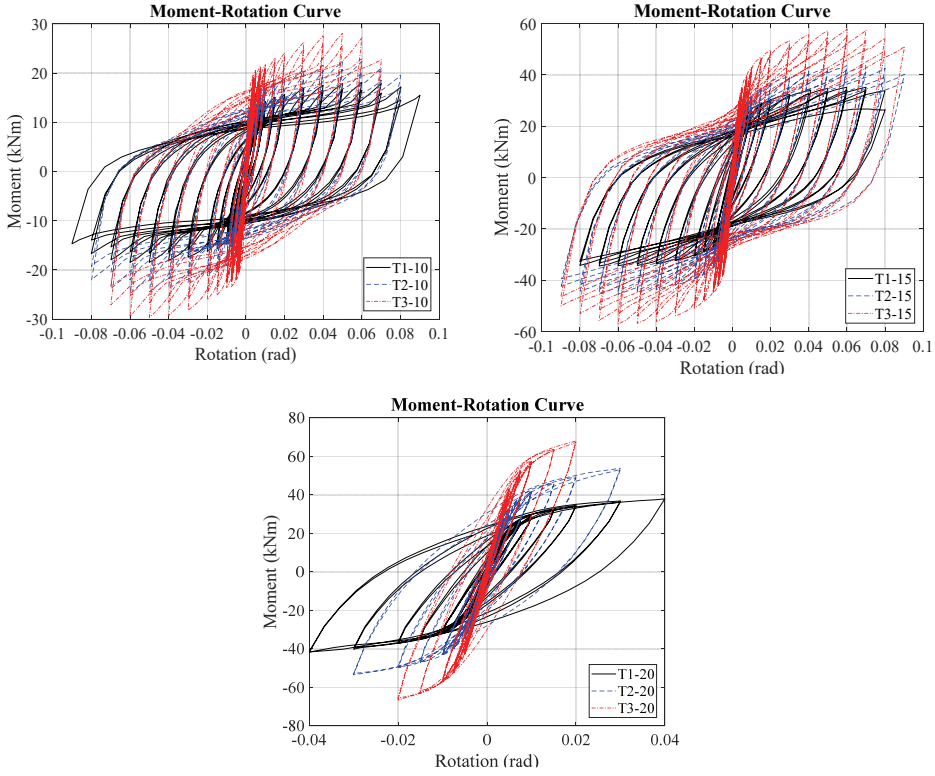

Figure 12 - Moment-rotation hysteretic loops at different end-plate height

3.3. Number of Bolt Rows

Figure 13 shows the moment-rotation curve of the connections having different end-plate configurations; with altogether 3, 4 and 5 with the thickness of 10 mm, 15 mm and 20 mm, respectively. The moment capacity of the joint increased when the number of bolt row increased for the end-plate with t=10 and 15 mm, because more bolt row provides more fixed points on the end-plate that leads to larger yielding capacity. However, effect of the number of bolt rows for the end-plate with t=20 mm was found to be negligible because beam web yielding governed the behavior of the joint.

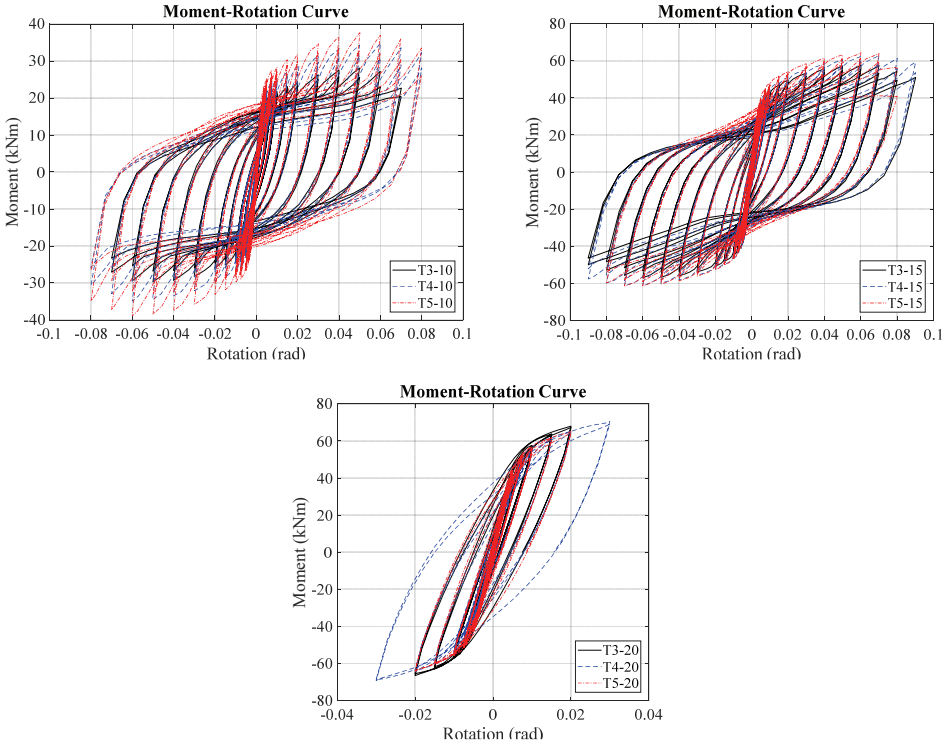

Figure 13 - Moment-rotation hysteretic loops for equal end-plate height with different numbers of bolt rows

3.4. Classification of the Connections according to Eurocode 3

Considering the stiffness, a connection can be classified as nominally pinned (NP), semi-rigid (SR) or rigid through the comparisons with EI_b/L_b, where E, I_b, and L_b are the modulus of elasticity, second moment of area and the span of the connected member. The span of the connected member will be taken as 3.14 m (twice of the span of the cantilever beam and if the tested specimen beam section size is applied in 6 m span frames, the ratio in Table 3 ($R_i/(E_bI_b/L_b)$) will be almost doubled). According to the Eurocode 3 (EN 1993-1-8, [13]), connections having end-plates of t=15 mm and t=20 mm (T3, T4, T5) transfer more than 25% of the beam plastic moment capacity. Therefore they are called partial-strength (PS) connection while the connection with end-plate of t=10 mm is classified as nominally pinned. Furthermore, the results indicate that all of the specimens are categorized as semi-rigid connections because the ratio of $R_i/(E_bI_b/L_b)$ is between 0.5 and 25. Finally, for sufficient rotation capacity, end-plate thickness should be limited. In this study, based on the experimental results, end-plate thickness of 15 mm was found to be critical thickness. Therefore, the connection with 20mm thick end-plate exhibited insufficient behavior in terms of ductility and rotation capacity.

Connection assessment in terms of maximum moment of the connection M_{max}, to the ratio of the plastic moment capacity of the beam and initial stiffness of the connection to the ratio of the flexural stiffness of the beam according to Eurocode 3 (EN 1993-1-8, [13]) is given in the Table 3.

Table 3 - Connection assessment based on Eurocode classification

	R_i (kNm/ rad)	$\frac{E_b I_b}{L_b}$	$\frac{R_i}{E_b I_b / L_b}$	M_{max} (kNm)	$M_{pl,IPE}$	$\frac{M_{max}}{M_{pl,IPE}}$	EC3 classfic.
T1-10	5494.0	5465.9	1.00	18.44	204.1	%9	SR/NP
T1-15	5471.1	5708.0	0.96	35.51	188.4	%19	SR/NP
T1-20	6179.3	5441.8	1.13	41.69	209.1	%20	SR/NP
T2-10	7078.0	5465.9	1.29	24.75	204.1	%12	SR/NP
T2-15	7386.0	5708.0	1.29	45.51	188.4	%24	SR/NP
T2-20	8355.0	5441.8	1.54	53.49	209.1	%26	SR/PS
T3-10	9667.1	5465.9	1.76	29.62	204.1	%15	SR/NP
T3-15	9792.9	5708.0	1.72	57.89	188.4	%31	SR/PS
T3-20	9755.6	5441.8	1.79	67.98	209.1	%33	SR/PS
T4-10	9481.3	5465.9	1.73	34.77	204.1	%17	SR/NP
T4-15	10122	5708.0	1.77	63.11	188.4	%34	SR/PS
T4-20	9402.2	5441.8	1.73	69.33	209.1	%33	SR/PS
T5-10	8962.9	5465.9	1.64	38.90	204.1	%19	SR/NP
T5-15	9825.2	5708.0	1.72	64.44	188.4	%34	SR/PS
T5-20	9708.5	5441.8	1.78	64.98	209.1	%31	SR/PS

Tests on the header end-plate connections revealed that the behavior of the specimens with the end-plate of t=15 mm and t=20 mm (T3, T4, T5) has satisfied requirements stipulated by the Eurocode 3 for partial strength and semi-rigid connections. The connections with 15 mm thick end-plate experienced rotation levels beyond 0.04 rad. However, the rotation capacity of the connection with end-plate thickness of t=20 mm was not more than 0.04 rad and they seem not to be suitable for use together with the special moment frames because this requires that the rotation capacity of the connection be at least 0.04 rad according to AISC provisions (AISC341-16, [17]). Additionally, the behavior of the connection was significantly improved with 15 mm thickness when compared to that with 10 mm thick header end-plate.

4. NUMERICAL INVESTIGATIONS ON HEADER-END PLATE CONNECTIONS

4.1. Flexural Resistance Based on the Obtained Yield Line Configurations

The flexural strength of the end-plate is determined by using yield line (YL) analysis which estimates the yield moment of the end-plate (Bruneau et al. [19]). For this purpose, based on the experimental and the FE analyses results, yield line pattern as shown in Figure 14, is determined and in order to obtain the flexural strength, the equality of the work done by the internal forces to that done by the external forces is generated.

General expression for internal work stored by the yield line pattern is as follows.

$$W_i = \sum_{n=1}^{N} (m_p \theta_{nx} l_{nx} + m_p \theta_{ny} l_{ny}) \tag{1}$$

Where θ_{nx} and θ_{ny} are the x and y components of the relative rotation of the rigid plate segments along the yield line. l_{nx} and l_{ny} are the x and y components of the yield line length and m_p is the plastic moment strength of the plate per unit length which is defined as below.

$$m_p = F_y \frac{t^2}{4} \tag{2}$$

Where t is the thickness and F_y is the actual yield strength of the end-plate (Table 1). For the samples of T4-10 and T5-10, the total internal work W_i stored in the yield lines can be calculated with Eq. 3, and external work W_e, due to external moment M, can be calculated with Eq. 4.

$$\begin{aligned} W_I &= m_p \times g \times [\frac{h_1}{m_f} + \frac{h_2}{p_f} + \frac{h_2}{s}] \times \theta^\circ + ... \\ &... + 8 \times m_p \times [(g_p + m_f) \times \frac{h_0}{g} + (p_f + s) \times \frac{h_2}{g} + 0.5(p_f + m_f) \frac{h_0 + h_2}{2g}] \times \theta^\circ \end{aligned} \tag{3}$$

$$W_e = \frac{M}{h} \theta h \tag{4}$$

Where M_{pl} is the end plate flexural strength and θ is the applied virtual displacement that is equal to $1/h$, where h is the height of the end-plate. Besides, g, h_0, h_1, h_2, p_f, g_p, m_f and s are the distances that define the geometric properties of the end-plate as shown in Figure 14.

In the FE models and the tests, the actual material properties have been used while the effect of the strain hardening has not been considered in the yield line analysis. Therefore, flexural capacities M_{pl}, from yield line method indicates the level of the moment at the beginning of

the plastification of the connection obtained by the FE method and experimental tests as shown in Figure 19. The flexural capacity value and end-plate yield line mechanism parameter Y_p are given in Table 4, obtained by the following equations;

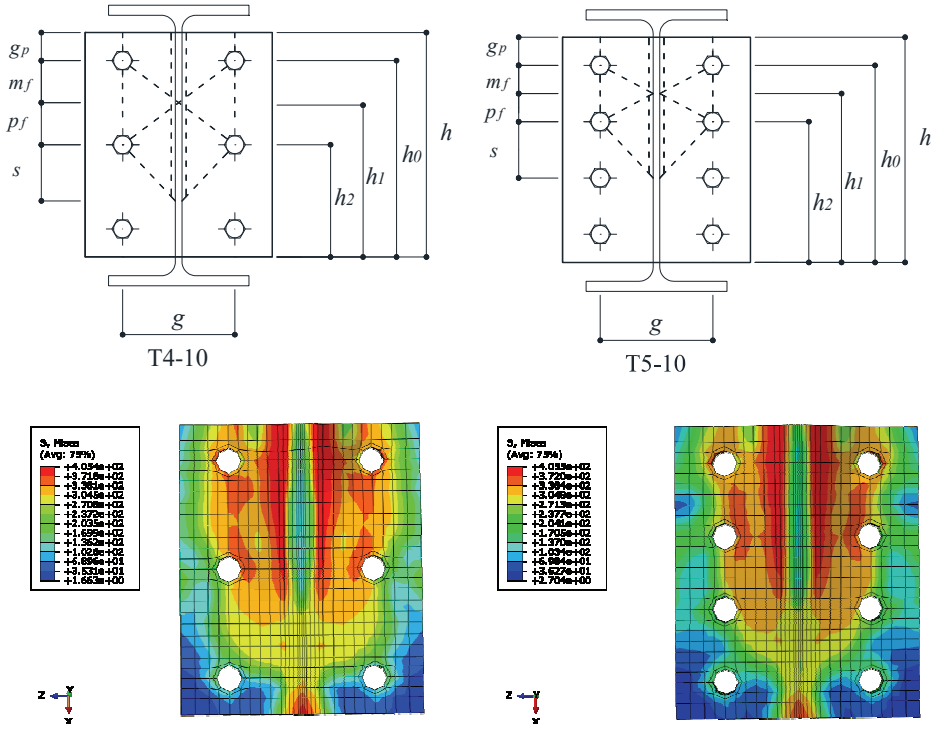

Figure 14 - Yield line patterns and Stress contour diagram (FE results) of end-plates of T4-10 and T5-10

$$M_{pl} = F_y \times t^2 \times Y_P \tag{5}$$

$$Y_P = \frac{g}{4}\left[\frac{h_1}{m_f} + \frac{h_2}{p_f} + \frac{h_2}{s}\right] + 2\left[(g_p + m_f) \times \frac{h_0}{g} + (p_f + s) \times \frac{h_2}{g} + 0.5(p_f + m_f)\frac{h_0 + h_2}{2g}\right] \tag{6}$$

$$\frac{\partial W}{\partial s} = 0 \rightarrow s = \frac{g}{2\sqrt{2}} \tag{7}$$

Table 4 - Moment capacity (YL) of the connections with 10mm thick plate

Specimen	t (mm)	Y_p	F_y (N/mm^2)	M_{pl} (kNm)
T4-10	10	835.96	287	23.98
T5-10	10	917.13	287	26.31

To limit the complexity of the equations, the plate material removed by drilling bolt holes is not considered and beam web thickness is taken to be zero as presented in Murray and Sumner [20].

4.2. Mechanical Model

In order to understand and to represent the elastic behavior of the connection before yielding, the initial stiffness of the connection must be known. Herein, initial stiffness of the end-plate connections can be estimated according to Faella et al. [21] based on the simulation of the connection by using a set of rigid or flexible components. It is easy to recognize that the prediction of the joint behavior involves the following components:

- Column web in shear (cws)
- Column web in compression (cwc)
- Column flange in bending (cfb)
- End-plate in bending (epb)
- Bolts in tension (bt)
- Column web in tension (cwt)
- Beam flange and web in compression (bfc)
- Beam web in tension (bwt)

For the extended and flush end-plate connections, the first six components govern the flexural resistance and initial rotational stiffness. Conversely, the last two components must be considered in the evaluation of the joint flexural resistance only. However, beam web strains control the initial stiffness of the header end-plate connections. Therefore, for the initial stiffness of the header end-plate connection, beam web in tension must be taken into consideration as an elasto-plastic spring component as shown in Figure 15. The effect of the beam flange and web in compression can be neglected for rotational stiffness of the connection.

The evaluation of the initial stiffness requires a knowledge of the effective stiffness coefficient of the first tension bolt row that is obtained by a set of springs in series. Then, the initial stiffness $S_{j,ini}$ can be determined through the Eq. 8 where K_i is the stiffness coefficient representing i component and h_z is the lever arm. Translational stiffness of the other bolts were ignored.

$$S_{j,ini} = \frac{h_z^2}{\frac{1}{K_{cwt}} + \frac{1}{K_{cfb}} + \frac{1}{K_{epb}} + \frac{1}{K_{bwt}} + \frac{1}{K_{bt}} + \frac{1}{K_{cws}} + \frac{1}{K_{cwc}}} \quad (8)$$

As a result, initial stiffnesses of the specimens T5-10, T5-15 and T5-20 are 9122 kNm/rad, 9780 kNm/rad and 10047 kNm/rad, respectively. These values proved to be a close approximation of the experimental results of 8962.9 kNm/rad, 9825.2 kNm/rad and 9708.5 kNm/rad, respectively.

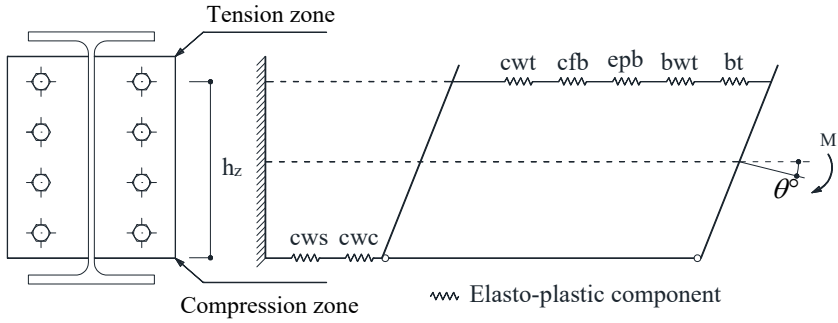

Figure 15 - Characterization of the beam-to-column joints components

4.3. Finite Element Model

In order to identify the effect of different parameters on the behavior of connection and to understand important local effects which are difficult to measure with sufficient accuracy, 3-D FE models which account for both geometrical and material nonlinearities were developed using the multi-purpose software package ABAQUS [22] (Figure 16). To simulate the projected test setup, the column was assumed to be pin connected at the ends and the lateral displacement of the column was prevented. A point load was applied to tip of the beam (To reference point, X^{RP-1} in Figure 16) which is allowed to deflect horizontally in x-direction in the same manner as in the test. The beam was laterally supported to prevent any possibility of premature failure caused by lateral torsional buckling, as done in the tests.

For more reliable performance, the eight-node brick elements C3D8I with incompatible modes are used. Since having additional degree of freedoms, C3D8I has the capability to capture bending behavior better. Modelling the contact interaction; between the outer surfaces of the column flange and header end-plate and between the bolt head/nut and column flange/end-plate requires two different interaction properties. First one is 'hard contact' property and the second one is tangential behavior of the contact. The friction coefficient between the contact surfaces was taken as 0.30. Also, to get acceptable results under flexural moment, at least four layers were formed through the member thickness in element meshing. The optimal solution is to use a fine mesh in areas of high stress and a coarser mesh in the remaining areas. Hexagonal bolt heads and nuts are idealized as circular bolt heads and nuts

to simplify the model and washers are not modeled. Bolt holes are assumed to be 2 mm larger than the nominal bolt diameter (d_b=20 mm). The FE analyses of the model were done using two load steps. The first load step was to apply pretension forces to the bolts by applying displacements to the ends of the bolts. The prescribed bolt displacements corresponding to the axial force of 172 kN were calculated considering axial rigidity of the bolts. The second load step was employed to define cyclic loading path applied by imposing horizontal displacement to the free end of the beam. The available material test data was in the form of engineering stress and strain. Therefore, in the FE models the material data converted from engineering stress σ_{eng} and strain ε_{eng} to true stress σ_{true} and strain ε_{true} based on the following equation. The plasticity behavior in the joint was represented by the combined hardening assumption and Von Mises yield criterion. Figure 17 and Figure 18 display the deformed shape of the connections at the maximum target displacement (0.07, 0.08 and 0.02 rad rotation for specimens; T5-10, T5-15 and T5-20, respectively) and equivalent plastic strain distributions at the end of the FE analysis, respectively. Quantitative comparison in terms of bending strength and initial stiffness between the experimental and the simulated capacity is given in Figure 19. When the force applied at the end of the beam is a push force, the rotation is negative, and in case of pull force, the rotation is positive in the given moment-rotation curves.

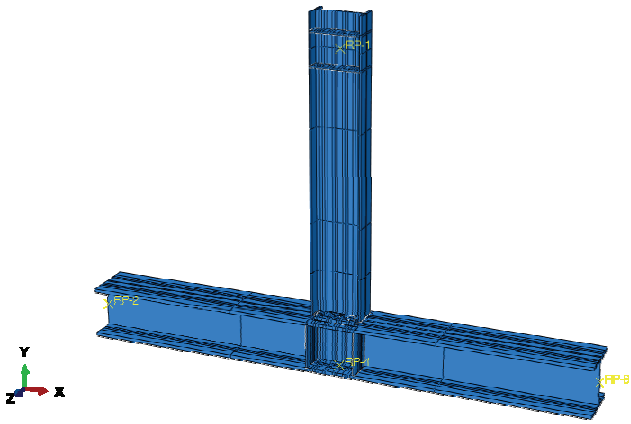

Figure 16 - 3D FE model in ABAQUS (T5-15)

$$\sigma_{true} = \sigma_{eng}(1+\varepsilon_{eng}); \qquad \varepsilon_{true} = \ln(1+\varepsilon_{eng}); \tag{9}$$

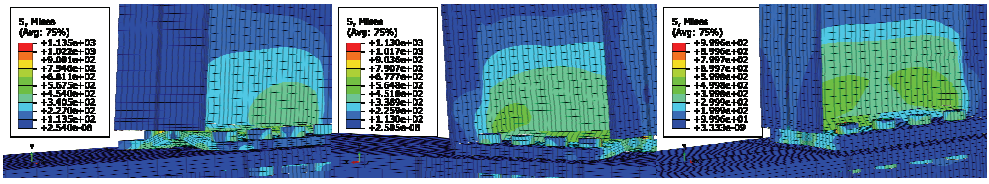

T5-10 T5-15 T5-20

Figure 17 - Stress contour diagram and deformed shape of the specimens T5

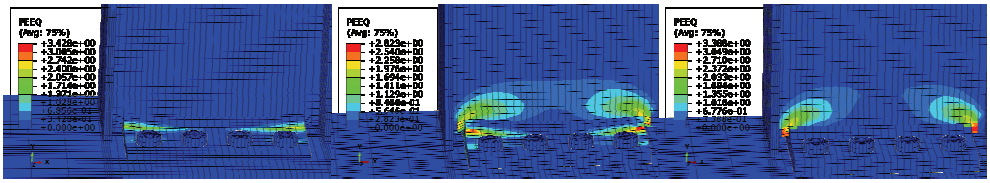

T5-10 T5-15 T5-20

Figure 18 - Equivalent plastic strain distributions for the specimens T5

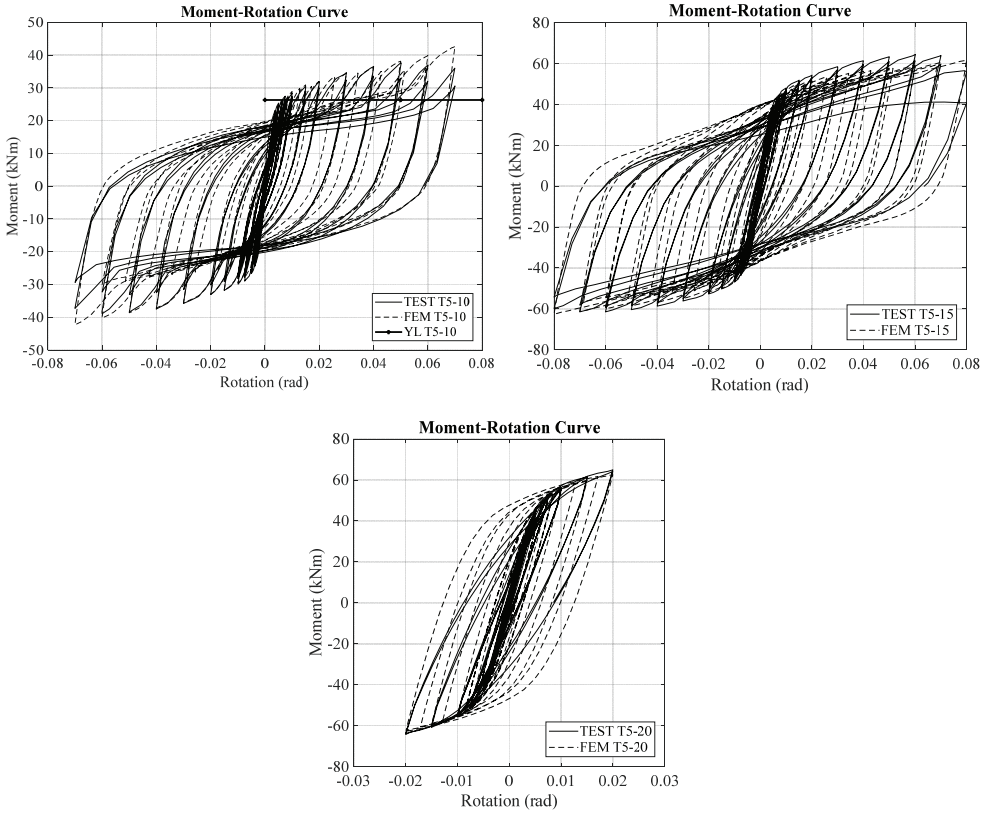

Figure 19 - Comparison of the FE model and experimental test results

It can easily be seen that, the achieved numerical results provided satisfactory agreement with the experimental test results. Although of the high accuracy of the results obtained, the main defect that the inability of FE model to reflect the stiffness deterioration in hysteretic loops as in the actual test behavior of the specimen T5-20, because the decrease in the stiffness due to yielding of the beam web at the connection could not exactly be represented in the FE model.

Equivalent plastic strain (PEEQ) index was employed to measure inelastic strain demands which are defined as the ratio of the equivalent plastic strain to the yield strain. PEEQ index for the end-plate of the specimen T5-20 is very less compared to the end-plates of the T5-10 and T5-15. In this basis, it can be stated that by use of thin or intermediate end-plates, the potential of ductile behavior provided by plastic hinge formation within the end-plate increases when compared to the connections with thick plates.

4.4. Recommendation to Determine the Critical Thickness

Based on the test results, the behavior of header-end plate connections is controlled by two limit states such as end-plate tearing and rupture of the beam web. According to this study, thin plate behavior should be adopted to ensure that the connections have enough rotation capacity under cyclic loading when more energy dissipation, as expected from a structural system, is intended during the earthquakes. A limit for header-end plate thickness, called critical thickness, should be defined to distinguish between thick and thin end plate behaviour. Critical thickness, t can be determined by ensuring that the flexural capacity of end-plate is smaller than that of the portion of the beam web which is effective in bending (Eq.10).

$$F_y \times t^2 \times Y_P \le F_{ybw} \times \frac{t_w \times h_{eff}^{\ 2}}{4} \qquad h_{eff} \cong 1.23 \times h \le d_b \tag{10}$$

$$t \le \sqrt{\frac{0.38 \times h^2 \times F_{ybw} \times t_w}{F_y \times Y_P}} \tag{11}$$

In which, h_{eff} is the height of beam web which is assumed to be effective in bending based on the experimental and FE analyses results. F_y and F_{ybw} are actual yield stresses of end plate and beam web material, respectively. Thickness of end plate and of beam web are designated by t and t_w, respectively.

5. CONCLUSIONS

Sixteen specimens with different header end-plate configurations have been tested under cyclic loading in order to investigate the actual behavior of the header end-plate connections. Detailed FE analyses were also carried out to support the investigation. The parameters considered were the thickness of the end-plate, height of the end-plate and the number of bolt rows. According to the test results, the following conclusions can be drawn:

End-plate thickness has remarkable influence on the hysteretic behavior of the connections. The relatively thick end-plate connections (in this study, t=20mm) have higher flexural capacity. However, the energy dissipation capacities are limited due to premature rupture of the beam web that occurred when the Von Mises stresses reached to ultimate stress of the

beam web. Therefore, the increase in the end-plate thickness did not result in an increase in the connection ductility. The specimen having t=15 mm thick end-plate has stable hysteretic loops and energy was dissipated by flexural behavior of the end-plate and beam web. If the end-plate thickness is relatively thin the connection can be called nominally pinned. As long as the thinner and intermediate end-plates were employed, prying forces which increase the tensile stresses in the bolts became more pronounced.

Since the amount of end plate cross-sectional area in yielding along the folding lines is not significantly increased with increasing bolt rows, the effect of using more bolt rows on the behaviors of the connections with thin and intermediate end-plates has been found small. However, it is found that increasing the bolt row has no effect on the connections with thick plates because the failure mode of the connections has been controlled by the rupture of the beam web. Moreover, for the same thickness, increasing the depth of the connection has shown enhanced capacity for all types of the end-plate configurations. It is also noticed that the stiffness of the connection increases with the increase in the depth of the end-plate.

Tests on the header end-plate connections showed that the actions of the specimens with the end-plate thickness t=15 mm and t=20 mm (T3, T4, T5) met the Eurocode 3 criteria for partial strength and semi-rigid connections. However, the specimens with a thickness of the end-plate t=20 mm do not have sufficient rotational capacity.

Additionally, finite element model results have shown good correlation with the experimental results and were proven to simulate the behavior of the connection effectively. Yield moment capacity of the header end-plate connection attained by the tests and FE analysis under cyclic loading was compared by the results obtained based on the yield line theory.

A mechanical model was proposed for obtaining rotational stiffness of the connection. In the measurement of the rotational stiffness, the response of the beam web controlling the initial stiffness of the header end-plate connections must be considered in the mechanical model.

From the above discussion, it is suggested that for the header end-plate connections in bending, it is necessary to limit the thickness of the end-plate in order to avoid brittle failure of beam web and to obtain ductile joints by yielding of the end-plate in bending. This can be accomplished by designing the end plate whose flexural capacity is smaller than that of the effective cross-section in bending within the beam web. If it is so, such connections also would help to dissipate energy imposed by earthquakes.

Symbols

bfc	:	Beam flange and web in compression
bt	:	Bolts in tension
bwt	:	Beam web in tension
cfb	:	Column flange in bending
cwc	:	Column web in compression
cws	:	Column web in shear

cwt	:	Column web in tension
d_b	:	Beam web depth
E	:	Modulus of Elasticity (N/mm^2)
epb	:	End-plate in bending
F_u	:	Actual tensile strength of the material (N/mm^2)
F_{ub}	:	Tensile strength of the bolt material (N/mm^2)
F_y	:	Actual yield stress of the end-plate (N/mm^2)
F_{yb}	:	Yield strength of the bolt material (N/mm^2)
F_{ybw}	:	Actual yield stress of the beam web (N/mm^2)
$g, h_0, h_1, h_2, p_f, g_p, m_f, s$	:	The distances that define the geometric properties of the end-plate
h	:	Height of the end-plate
h_{eff}	:	Height of the effective region within beam web in bending
h_z	:	Lever arm of the end-plate
I_b	:	Second moment of area of the connected member
K_i	:	Stiffness coefficient representing *i* component
l_{nx} , l_{ny}	:	x and y components of the yield line length
L_b	:	Span of the connected member
m_p	:	Plastic moment strength of the plate per unit length
M	:	External moment
M_{max}	:	Maximum moment attained just before failure in the tests
M_{pl}	:	Flexural strength capacity of end plate
NP	:	Nominally-Pinned
PS		Partial-Strength
R_i	:	Initial stiffness of the connection (Test results)
SR	:	Semi-Rigid
$S_{j,ini}$	:	Initial stiffness of the connection according to Eurocode 3
t	:	End-plate thickness
t_w	:	Beam web thickness.
W_e	:	External work due to external moment

W_i	:	Total internal work stored in the yield lines
Y_p	:	End-plate yield line mechanism parameter
ε_{eng}	:	Engineering strain
ε_{true}	:	True strain
θ	:	Applied virtual displacement
θ_b	:	Drift angle (relative displacement of beam divided by arm length)
θ_{max}	:	maximum connection rotation attained before failure
θ_{nx}, θ_{ny}	:	x and y components of the relative rotation of the rigid plate segments
σ_{eng}	:	Engineering stress
σ_{true}	:	True stress
ϕ (d_b)	:	Nominal bolt diameter (mm)

Acknowledgments

This research was financially supported by Research Fund of the Istanbul Technical University. Project Number: 41573

References

[1] Chen, W., Kishi, N. and Komuro, M., Semi-Rigid Connections Handbook, J. Ross Publishing, U.S.A, 2011.

[2] Sherif, H.M.H., Hazem, M. R., M. Nabil, A. and Sherif, A. M., Experimental study of prequalified status of flush end plate connections, Journal of Housing and Building National Research Center, HBRC journal, 12, 25-32, 2014.

[3] Bing, G., Qiang, G. and Feng, L., Experimental Behavior of Stiffened and Unstiffened End-Plate Connections under Cyclic Loading, Journal of Structural Engineering ASCE, 132(9), 1352-1357, 2006.

[4] Ismail, R.E.S., Fahmy, A.S., Khalifa, A.M. and Mohamed, Y.M., Numerical study on ultimate behavior of bolted end-plate steel connections, Latin American Journal of Solids and Structures, 13(1), 1–22, 2016.

[5] Haghollahi, A. and Jannesar, R., Cyclic behavior of bolted extended end-plate moment connectionswith different sizes of end plate and bolt stiffened by a rib plate, Civil Engineering Journal, 4(1), 200-211, 2018.

[6] Fang, C., Yam, M.C.H., Lam, A.C.C. and Xie, L., Cyclic performance of extended end-plate connections equipped with shape memory alloy bolts, Journal of Constructional Steel Research, 94, 122–136, 2014.

[7] Dessouki, A.K., Youssef, A.H. and Ibrahim, M.M., Behavior of I-beam bolted extended end-plate moment connections, Ain Shams Engineering Journal, 4, 685-699, 2013.

[8] Adey, B.T., Extended End Plate Moment Connections under Cyclic Loading, Master's thesis, University of Alberta, Alberta, Canada, 1997.

[9] Johnstone, N.D., Walpole, W.R., Behavior of steel beam-column connections, made using bolted end plates, Bulletin of the New Zealand National Society for Earthquake Engineering, 15(2), 82-92, 1982.

[10] AISC, Load and Resistance Factor Design Specifications for Structural Steel Buildings, 2nd Edition, American Institute of Steel Construction; Chicago, USA, 1994.

[11] Kishi, N., Komuro, M. and Chen, W., Four-parameter power model for Moment-rotation curves of end-plate connections, ECCS/AISC Workshop Connections in Steel Structures V, (c), 99–110, Amsterdam, The Netherlands, 2004.

[12] Jaspart, J.P., Demonceau, J.F., European design recommendations for simple joints in steel structures, Journal of Constructional Steel Research, 64, 822-832, 2008.

[13] EN 1993-1-8:2005, Eurocode 3: Design of Steel Structures-part 1-8: Design of Joints, European Committee for Standardization; Brussels, Belgium, 2005.

[14] Sommer, W.H., Behaviour of Welded Header Plate Connections, Master's thesis, University of Toronto, Toronto, Canada, 1969.

[15] Aggarwal, A.K., Behaviour of flexible end plate beam-to-column joints, Journal of Constructional Steel Research, 16, 111–134, 1990.

[16] Pilgr, M., Experimental verification of actual behaviour of header plate connections, The Nordic Steel Construction Conference, 2009.

[17] AISC 341-16, Seismic provisions for structural steel buildings, American Institute of Steel Construction; Chicago, IL, USA, 2016.

[18] TCDCSS, Turkish code for design and construction of steel structures 2016, Ministry of Environment and Urbanization; Ankara, Turkey, 2016.

[19] Bruneau, M., Uang, C.M. and Sabelli, R., Ductile Design of Steel Structures, (2nd Edition), McGraw Hill, New York, USA, 2011.

[20] Murray, M. and Sumner, E.A., Design Guide 4 Extended End-Plate Moment Connections Seismic and Wind Applications, (2nd Edition), American Institute of Steel Construction, Chicago, 2003.

[21] Faella, C., Piluso, V. and Rizzano, G., Structural Semi-Rigid Connections, Design and Software. Boca Raton FL: CRC Press LLC, USA, 2000.

[22] ABAQUS 2017, Dassault Systemes Simulia Corp., Abaqus/CAE User's Guide, Providence, RI, USA.